Large-scale molecular-dynamics simulation of nanoscale hydrophobic interaction and nanobubble formation

Takahiro Koishi[a)]
Innovative Nanopatterning Research Laboratory, Rikagaku Kenkyusho (RIKEN), Hirosawa 2-1, Wako, Saitama 351-0198, Japan

Kenji Yasuoka
Department of Mechanical Engineering, Keio University, Yokohama 223-8522, Japan

Toshikazu Ebisuzaki
Ebisuzaki Computational Astrophysics Laboratory, Rikagaku Kenkyusho (RIKEN), Hirosawa 2-1, Wako, Saitama 351-0198, Japan

S. Yoo and X. C. Zeng[b)]
Department of Chemistry, University of Nebraska - Lincoln, Nebraska 68588

(Received 6 June 2005; accepted 8 September 2005; published online 21 November 2005)

We performed large-scale molecular-dynamics simulation of nanoscale hydrophobic interaction manifested by the formation of nanobubble between nanometer-sized hydrophobic clusters at constrained equilibrium. Particular attention is placed on the tendency of formation and stability of nanobubbles in between model nanoassemblies which are composed of hydrophobic clusters (or patches) embedded in a hydrophilic substrate. On the basis of physical behavior of nanobubble formation, we observed a change from short-range molecular hydrophobic interaction to midrange nanoscopic interaction when the length scale of hydrophobe approaches to about 1 nm. We investigated the behavior of nanobubble formation with several different patterns of nonpolar-site distribution on the nanoassemblies but always keeping a constant ratio of nonpolar to polar monomer sites. Dynamical properties of confined water molecules in between nanoassemblies are also calculated. © *2005 American Institute of Physics*. [DOI: 10.1063/1.2102906]

I. INTRODUCTION

Hydrophobic interactions play an important role in the formation of detergent micelles, self-assembly of lipid membranes,[1] and conformational changes of biopolymers such as protein folding.[2–7] Among molecular-sized hydrophobes, such as nonpolar methane molecules, hydrophobic interaction is mainly originated from entropy effects through reorganization of near-hydrophobe water molecules.[8–14] On the other hand, among mesoscopic-or macroscopic-sized hydrophobes, e.g., between two planar hydrophobic surfaces, hydrophobic interaction can be induced by dewetting transition or capillary cavitation,[15–19] or by the formation of vicinal microbubbles[20–22] and inverted clathratelike structures.[23,24] The crossover from molecular to macroscopic like hydrophobic interaction was predicted to occur at about 1 nm length scale of the size of hydrophobes.[25,26] Much attention has been given to molecular and macroscopic hydrophobic interactions, however, physical behavior of nanoscopic hydrophobic interaction especially at the crossover regime is still less studied.[25–32] By means of large-scale molecular-dynamics (MD) simulations and using one of the fastest computers today,[33,34] we have attained some molecular-level insight into physics of the nanoscopic hydrophobic interaction.[35] Several physical features of nanoscopic hydrophobic interaction have been identified, which appear to differ dramatically from molecular hydrophobic interaction. Among others, a key feature that manifests the nanoscopic hydrophobic interaction is the formation of stable nanobubbles in between nanometer-sized hydrophobes when the hydrophobes can be held fixed (i.e., held in a constrained equilibrium condition). Other important features include that the range of nanoscopic interaction can extend beyond 1 nm, about twice of the interaction range of typical molecular hydrophobic interaction. When the length scale of hydrophobes is greater than 2 nm, the nanobubble formation exhibits hysteresis behavior, resembling macroscopic first-order transition.

The purpose of this paper is threefold: (1) to present more detailed information on the hydrophobic model system reported previously in a short letter,[35] particularly the information about the degree of hydrophobicity (via contact angle measurement) for the model hydrophobes; (2) to report MD simulation results on the tendency and stability of nanobubble formation in between sub-nanometer-sized hydrophobes; and (3) to investigate how the nanobubble formation is affected by changing pattern of nonpolar-site distribution on the model nanoassemblies, but keeping the same ratio of nonpolar to polar monomer sites. Some dynamical properties of confined water molecules in between two nanoassemblies are also computed.

[a)]Electronic mail: t-koishi@riken.jp
[b)]Electronic mail: xzeng@unlserve.unl.edu

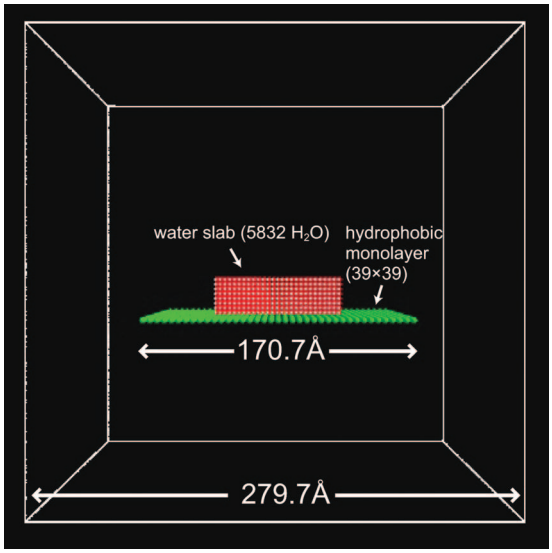

FIG. 1. (Color) A side view of the simulation system for calculating contact angle of microdroplet of water. An initial water configuration is a flat water slab (in red color) on a model hydrophobic monolayer (in green color) where each monomer site is modeled by a unit-atom CH_3 group.

II. SIMULATION SYSTEMS AND METHODS

A. System for calculating contact angle of microdroplet

The system consists of a rigid hydrophobic monolayer and a microdroplet of water, as shown in Fig. 1 where the initial configuration of the water droplet is simply a flat water slab (red color). The simulation box is a cube with a length of 279.7 Å. The popular SPC/E (Ref. 36) model was used for the simulation of water droplet. The hydrophobic monolayer is a rigid assembly of 39×39 nonpolar monomer sites (green color), where each monomer site is a CH_3 group modeled by the united-atom optimized potential for liquid simulation (OPLS).[37] The same water and nonpolar monomer-site models were also used in our previous simulation.[35] The SPC/E model potential includes two terms, a Coulomb term and a Lennard-Jones (LJ) term. The OPLS model of CH_3 group is simply a LJ particle. The parameters of LJ potential (ε and σ) for both models are listed in Table I. For the hydrophobic monolayer, the nearest-neighbor monomer site-site distance is 4.39 Å ($=2^{1/6}\sigma_{CH_3}$).

As mentioned above, the initial configuration of water microdroplet is an artificial one with a rectangular slab shape. The water slab contains $8\times27\times27=5832$ water molecules. To assure that the shape of equilibrated water droplet is independent of initial water configurations, another two artificial water configurations were considered: a cubic block of water with $18\times18\times18=5832$ water molecules and a vertical slab of water with $32\times13\times14=5824$ water molecules. The MD simulation was carried out at constant-volume and constant-temperature (298 K) condition. The Nosé-Hoover's method was used to control the temperature. The periodic boundary condition was applied in all three spatial dimensions. For all simulations with different initial water configurations, the system reached (vapor-liquid) equilibrium after about 200 ps. Another 200 ps simulation was then carried out for the purpose of measuring contact angle of the microdroplets. Note that the MD time step was set at 1.0 fs.

TABLE I. LJ parameters of oxygen site of SPC/E water and unit-atom site of OPLS CH_3.

	σ(Å)	ε(kcal/mol)
SPC/E	3.166	0.1553
OPLS CH_3	3.910	0.1600

B. System for simulation of nanobubble formation

The simulation system is nearly identical to the one used in the previous study.[35] A side view of the system is shown in Fig. 2. The size of simulation box was $472\times118\times59$ Å^3. About a half of the box is occupied by a water slab (in red-white color) while the other half is vapor (in black color). The water slab contains 54 224 water molecules with a total of 163 342 atomic sites. Two hybrid polar/nonpolar nanoassemblies are held fixed in the center of the water slab. The polar monomer sites of the nanoassemblies are simply SPC/E water molecules with a fixed center-of-mass position but allowed to rotate. The nonpolar monomer sites (in green color) are CH_3 group modeled by the united-atom OPLS, as mentioned above. The total number of polar and nonpolar sites on one nanoassembly is 169 ($=13\times13$). The ratio of the number of polar sites to nonpolar sites was fixed at 83/86 while the pattern of nonpolar-site distribution can be changed. In any cases, the patterns on the two nanoassemblies mirror one another. The nearest-neighbor monomer site-site distance (regardless of polar or nonpolar site) is 4.39 Å ($=2^{1/6}\sigma_{CH_3}$). The internanoassembly distance is fixed at 7.1 Å during the simulation so that about one water layer can be accommodated in between the two nanoassemblies.

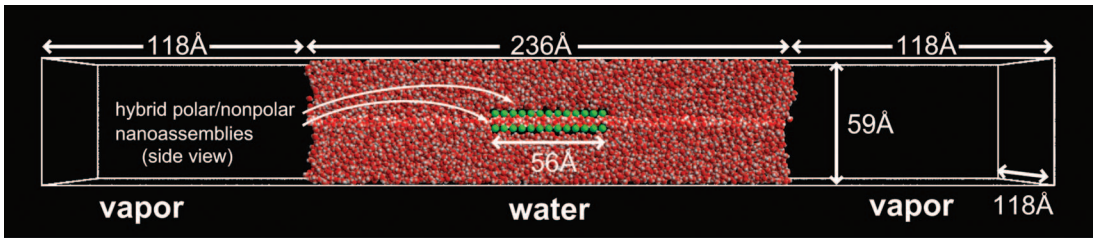

FIG. 2. (Color) A side view of the simulation system for study of nanobubble formation in between two hybrid hydrophobic/hydrophilic nanoassemblies. The two nanoassemblies (green color) are held fixed in parallel at the center of a water slab (in red and white color). Half of the simulation box is vapor which coexists with water. A top view of the nanoassemblies and snapshots of the highlighted water layer sandwiched in between two nanoassemblies are shown in Figs. 4–6.

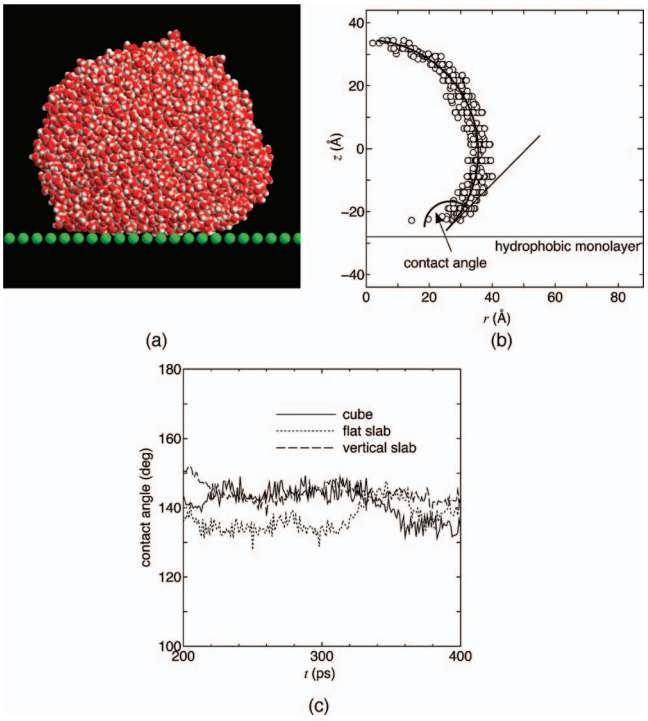

FIG. 3. (Color) (a) A snapshot of water microdroplet at $t=393$ ps. (b) Averaged equidensity surface in the radial direction (open circles) and the fitting surface (circular line) at MD time $t=393$ ps. The angle between the tangent line and the hydrophobic monolayer is defined as the contact angle. (c) Time dependence of calculated contact angles with three different initial water configurations (cubic, flat slab, and vertical slab).

Again, the MD simulation was carried out at constant-volume and constant-temperature (298 K) condition. Moreover, the system was maintained at the vapor-liquid coexistence so that the pressure of the system is only dependent on the temperature. The periodic boundary conditions were applied in all three spatial directions. The MD time step was set at 1.0 fs. Typically, the initial 50 000 MD time steps (50 ps) were used to equilibrate the system. During the equilibration run, all monomer sites of the nanoassemblies were set to be polar (hydrophilic). The long-range charge-charge interaction between the polar sites and water molecules was handled by using the Ewald method.

In both contact-angle and nanobubble-formation simulations, we used a special-purpose computer named Molecular Dynamics Machine (MDM).[33,34] The MDM has two types of nodes, the MDGRAPE-2 and WINE-2 nodes. The MDGRAPE-2 nodes handle calculation of the real-space part of the long-range charge-charge interaction as well as the van der Waals interaction. The WINE-2 nodes handle calculation of the reciprocal-space part of the long-range charge-charge interaction. Other computational duties are taken by a host computer, which include updating particle positions and evaluating temperature. The MDM has a peak speed of 78 Tflops, which was the fastest computer in 2004.

III. RESULTS AND DISCUSSION

A. Calculating contact angle of microdroplet

A snapshot of an equilibrated microdroplet in contact with the hydrophobic monolayer is shown in Fig. 3(a). To measure the contact angle of the microdroplet on the hydrophobic monolayer, we divided the entire simulation box into cubic meshes (with 5 Å length scale). We then calculated the local water density in each cubic mesh. An equi-local-density surface with a value of 0.016 $(=2/5^3)$ $Å^{-3}$ is regarded as the surface of the microdroplet since this local-density value is about a half of the density of bulk water. Figure 3(b) is a plot of averaged equidensity surface over the radial direction of the microdroplet. This averaged equidensity surface can be fitted by a line of circle. The angle between the tangent line of the fitting surface [see Fig. 3(b)] and surface of the hydrophobic monolayer is defined as the contact angle. At each MD step during the production run (200 ps), the contact angle was calculated and recorded. The results for three simulations with different initial water configurations are plotted in Fig. 3(c). It can be seen that the contact angle varies between 130° and 150° within the 200 ps MD simulation. A time averaged contact angle is about $142°\pm4°$, $137°\pm4°$, and $143°\pm10°$, respectively, based on the three MD simulations with cubic, flat-slab, and vertical-slab initial water configurations. The fact that these values of the contact angle are much larger than 90° indicates that the model monolayer is highly hydrophobic.

B. Tendency of formation and stability of nanobubbles between nanoassemblies

Four types of nonpolar-site patterns on the nanoassemblies were considered, including three checkerboard patterns and one randomly distributed pattern. For the three checkerboard patterns, the size of nonpolar checker cells (or nonpolar clusters) is mostly 3×3, or mostly 2×2, or 1×1, respectively. The side length of the 3×3 and 2×2 clusters is about 1.27 and 0.83 nm, respectively. As mentioned above, all nanoassemblies have the same ratio of nonpolar to polar site, which is a constant 83/86. The upper left panel in Figs. 4–6 displays a top view of model nanoassemblies with the 3×3 or 2×2 checkerboard pattern, or with randomly distributed nonpolar-site pattern. The latter was generated simply by randomly assigning polar and nonpolar sites without any correlation other than keeping the concentration ratio fixed. The next three panels in these figures display a series of snapshots of the water layer (highlighted in Fig. 2) in between two nanoassemblies. To view these snapshots from the top, the upper nanoassembly shown in Fig. 2 is removed. Therefore, if nanobubbles (or cavities) were formed in between the hydrophobes, one could see nonpolar sites (in green color) from the top.

With the 3×3 checkerboard nanoassemblies, the nanobubbles form spontaneously (typically within a few tens of picoseconds) in between the hydrophobes. This spontaneous nanobubble formation has been reported previously but with larger hydrophobes.[35] Moreover, once formed, the nanobubbles were all stable during the 500 ps MD simulation. Three snapshots of these nanobubbles at 100, 300, and 500 ps are shown in Fig. 4. These results suggest that the length scale of the 3×3 hydrophobic cluster (1.27 nm) seems sufficiently large to sustain a nanobubble. On the other hand, when the length scale of hydrophobic cluster is re-

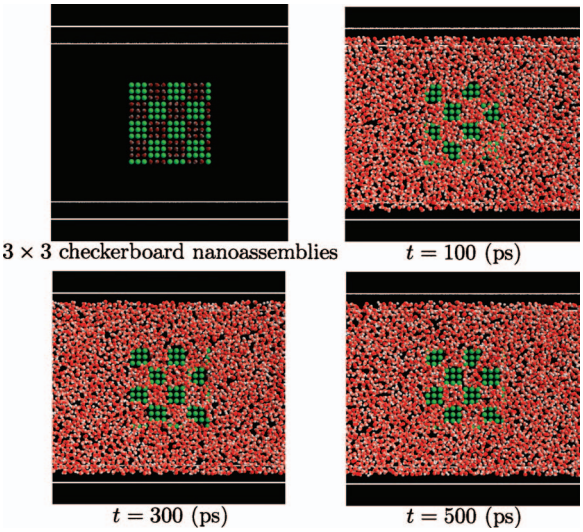

FIG. 4. (Color) The upper left panel is a top view of the 3×3 checkerboard nanoassembly. The nonpolar sites (in green color) are modeled by unit-atom CH_3 group and the polar sites are modeled by SPC/E water molecules. The other three panels are snapshots of the highlighted water layer shown in Fig. 2. To view the water configuration, the upper nanoassembly shown in Fig. 2 is removed. If nanobubbles form in between hydrophobes, one can see the green colored nonpolar sites of the lower nanoassembly shown in Fig. 2.

duced to 0.83 nm (2×2), although spontaneous nanobubble formation can still occur, the nanobubbles were no longer stable. The three MD snapshots shown in Fig. 5(a) at 100, 300, and 500 ps illustrate unstableness of the nanobubbles. Another evidence of this unstability of nanobubbles can be seen via calculating the local density of water in between a targeted 2×2 hydrophobic checker cell, as shown in Fig. 5(b). The fluctuation of the local density in between two hydrophobic clusters [highlighted by the white square in Fig. 5(a)] is indeed large. A nanobubble clearly forms at $t=100$ and 300 ps, but nearly disappears at $t=500$ ps. All these results indicate that the size of hydrophobic cluster (2×2) is too small to sustain a stable nanobubble and that the nanobubble state is much more stable in between two 3×3 hydrophobic clusters. As the size of hydrophobic cells was further reduced (1×1), namely, to molecular scale, nanobubbles were never observed within the time of the MD simulation, even the total number of nonpolar sites was unchanged.

For the nanoassemblies having randomly distributed nonpolar sites, four stable nanobubbles formed as highlighted by four white circles in Fig. 6. One can see from the upper left panel that at these circled locations, a minimum 2×3 nonpolar cell can be identified. Note that the area for a 2×3 nonpolar cluster is about 1 nm^2. It appears that this is the minimum surface area for hydrophobes to sustain a stable nanobubble. Thus, on the basis of physical behavior of nanobubble formation, we conclude that a change from short-range molecular hydrophobic interaction to midrange nanoscopic hydrophobic interaction may occur when the length scale of a hydrophobe reaches to about 1 nm.

As mentioned in the previous section, centers of the hydrophilic molecules (SPC/E water) on the nanoassemblies are held fixed but the molecules are allowed to rotate. In Fig. 7(a), we plot orientation distributions of these hydrophilic

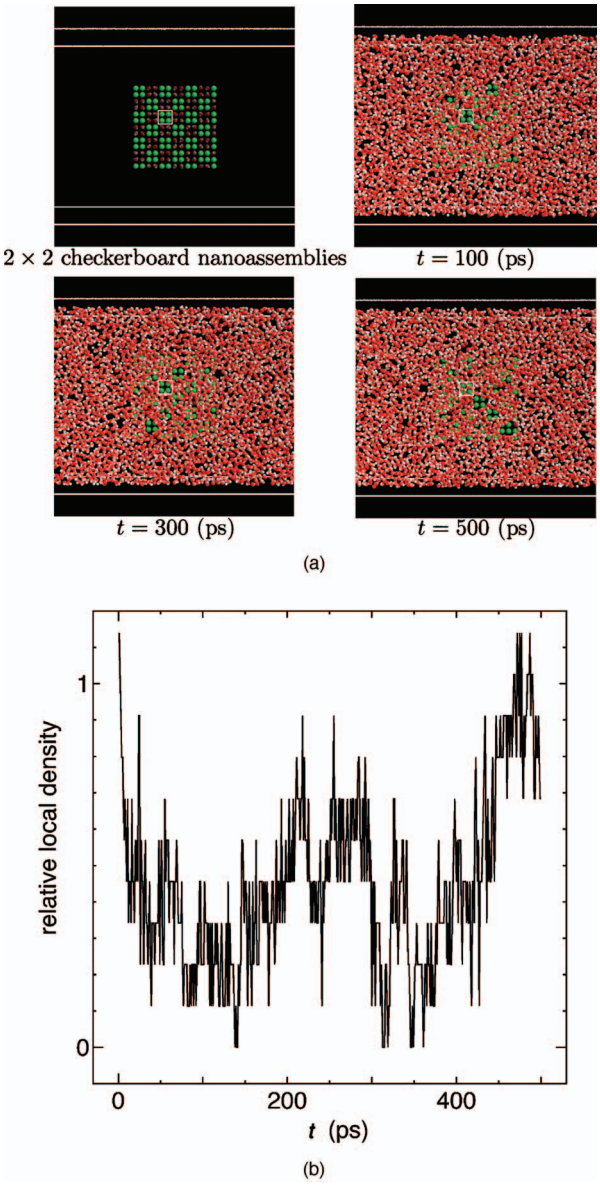

FIG. 5. (Color) (a) Same as Fig. 4 but for the 2×2 checkerboard nanoassembly. (b) Calculated relative local density within a small region highlighted by a white square in (a).

molecules in three cases of model nanoassemblies. The angle θ is defined between molecular dipole axis and the surface normal (z axis) of the lower nanoassembly. It can be seen that the dipole axis of the hydrophilic molecules have a higher probability to be in parallel or antiparallel with the surface normal, and this is true in all the three cases of model nanoassemblies. In Fig. 7(b), we plot site-site pair correlation functions between oxygen atoms (O_w) of the confined water molecules and polar sites (O_f) or nonpolar sites (CH_3), in the three cases of model nanoassemblies. One can clearly see a higher correlation (especially a higher second peak in the correlation functions) between these sites in the case of the 2×2 checkerboard model. This result suggests the existence of a higher local density of water in between the 2×2 model nanoassemblies. The time dependence of relative density, the density of water in between two nanoassemblies normalized by the density of bulk water, is shown in Fig. 7(c). It is

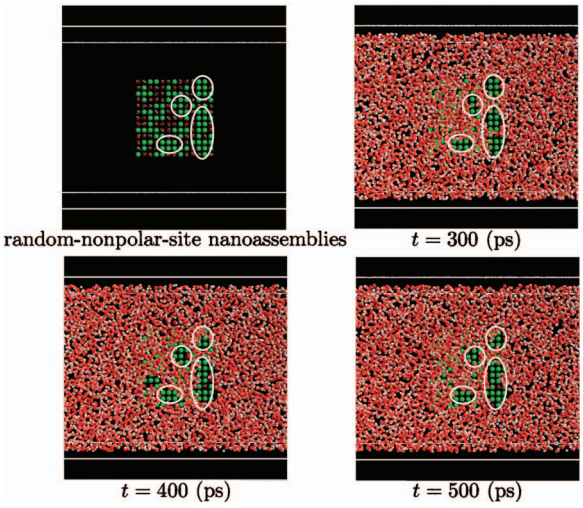

FIG. 6. (Color) Same as Fig. 4 but for the random-nonpolar-site nanoassembly. Four stable nanobubbles are highlighted by white circles.

expected that the relative density should decrease with increasing the total volume of nanobubbles. Thus, the fact that the relative density decreases with time in the case of 3×3 checkerboard and the random nonpolar-site nanoassembly indicates that nanobubbles were growing during the 500 ps MD run. However, in the case of the 2×2 checkerboard model, the relative density is more or less a constant but still appreciably smaller than 1.0. This result is consistent with the observation that the nanobubbles are unstable. Finally, it is interesting to note that the relative density in the case of the 1×1 checkerboard model is even greater than 1.0, that is, the local water density in between the nanoassemblies is

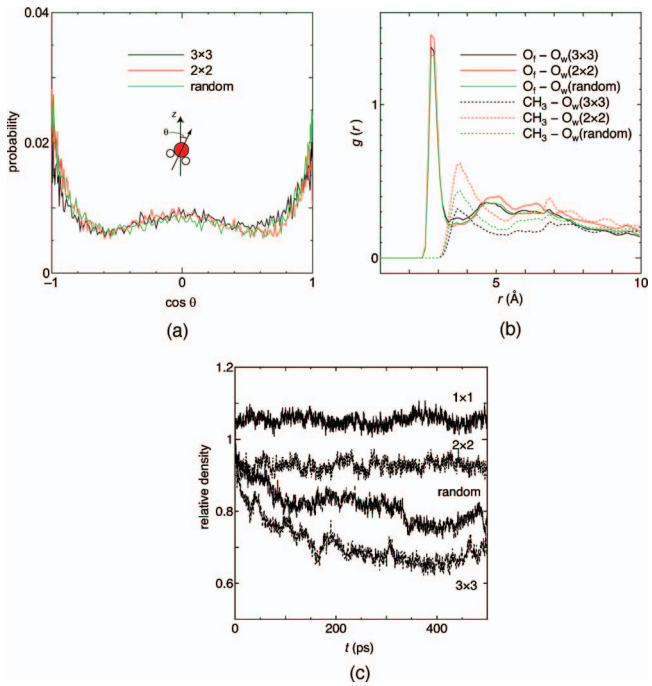

FIG. 7. (Color) (a) Orientation distributions of hydrophilic molecules on the nanoassemblies in the case of three model nanoassemblies. (b) Site-site pair correlation functions between oxygens (O_w) of the confined water and polar sites (O_f) or nonpolar sites (CH_3) on the nanoassemblies. (c) Time dependence of the relative densities of water in between various nanoassemblies.

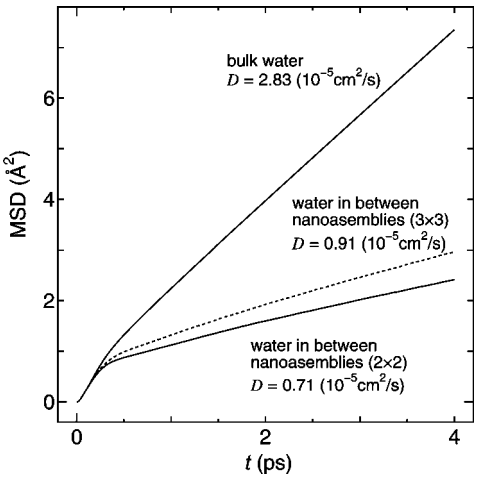

FIG. 8. The mean-square displacements (MSD) of water in between two nanoassemblies and MSD of bulk water.

even higher than the bulk density. Although the calculation of local density somewhat depends on the definition of local volume, the fact that the relative density is close to bulk water suggests that even with the same number of nonpolar sites, a uniform distribution of the nonpolar/polar sites (like in the case of the 1×1 checkerboard model nanoassemblies) may have little effects to the nanobubble formation, and thus giving no hydrophobic interaction. We conclude that the pattern of nonpolar-site distribution may play a bigger role than the total number of nonpolar sites as far as the nanobubble formation is concerned.

C. Dynamical properties of water molecules in between nanoassemblies

Dynamical behavior of water molecules in between two nanoassemblies can be studied through calculation of the diffusion constant and the velocity autocorrelation function. The diffusion constant of water molecules in between the two nanoassemblies $D_{\mathbf{in}}$ and that of bulk water $D_{\mathbf{out}}$ are computed based on calculation of the mean-square displacement given below:

$$D_{\mathbf{in}} = \lim_{t\to\infty}\frac{1}{6t}\langle|\mathbf{r}_{\mathbf{in}}(t) - \mathbf{r}_{\mathbf{in}}(0)|^2\rangle,$$
$$D_{\mathbf{out}} = \lim_{t\to\infty}\frac{1}{6t}\langle|\mathbf{r}_{\mathbf{out}}(t) - \mathbf{r}_{\mathbf{out}}(0)|^2\rangle, \quad (1)$$

where $\mathbf{r}_{\mathbf{in}}$ is the position of a water molecule in between two nanoassemblies and $\mathbf{r}_{\mathbf{out}}$ is the position of a water molecule outside of the two nanoassemblies. In Fig. 8, we plotted the mean-square displacements of water molecules in between 3×3 and 2×2 checkerboard nanoassemblies, respectively, as well as in the bulk water. The diffusion constants are given as legends of Fig. 8. In addition, the diffusion constant of water molecules in between the random nonpolar-site nanoassembly is $D=0.885\times10^{-5}$ cm^2/s. Interestingly, even the water in between two nanoassemblies entails nanobubbles, either more stable or less stable; the diffusion rate of water molecules is always slower in between nanoas-

TABLE II. Lifetime of hydrogen bond of water molecules in between two nanoassemblies.

	Lifetime of hydrogen bond (ps)	
	O_f-O_w	O_w-O_w
3×3	0.442	0.277
2×2	0.468	0.288
Random	0.424	0.283

semblies than in the bulk water. Furthermore, water molecules diffuse slightly slower in between the 2×2 checkerboard nanoassemblies than in between the 3×3 checkerboard nanoassemblies. Presumably, the more uniform nonpolar sites distribute (like in the 1×1 checkerboard model), the slower the translational diffusive motion of water molecules in between the nanoassemblies. To gain more insight into the diffusivity of confined water, we calculated averaged lifetime of hydrogen bonds in the confined water (i.e., water molecules between the two nanoassemblies) as well as that between the confined water and hydrophilic molecules on the nanoassemblies. The results are given in Table II. Note that here we used one geometry and one energy criterion to define a hydrogen bond, that is, if the intermolecular O–H distance is less than 2.2 Å, and if the interaction energy between the same two molecules is less than −10 kJ/mol, we assign a hydrogen bond between the two molecules. It can be seen from Table II that in all the three cases the averaged lifetime of hydrogen bond in the confined water is longer in the case of the 2×2 checkerboard model, followed by the random nonpolar-site model and the 3×3 checkerboard model.

The velocity autocorrelation functions of water molecules in between the two nanoassemblies $C_{\mathbf{in}}(t)$ and that of bulk water $C_{\mathbf{out}}(t)$ are also calculated based on the relations

$$C_{\mathbf{in}}(t) = \langle \mathbf{v}_{\mathbf{in}}(t) \cdot \mathbf{v}_{\mathbf{in}}(0) \rangle,$$
$$C_{\mathbf{out}}(t) = \langle \mathbf{v}_{\mathbf{out}}(t) \cdot \mathbf{v}_{\mathbf{out}}(0) \rangle, \tag{2}$$

where $\mathbf{v}_{\mathbf{in}}$ is the velocity of a water molecule in between two nanoassemblies and $\mathbf{v}_{\mathbf{out}}$ is the velocity of a water molecule outside of the two nanoassemblies. In Figs. 9(a) and 9(b), we plotted, respectively, the velocity auto-correlation functions $C(t)$ and the density of states of intermolecular vibrational motion $\tilde{C}(\omega)$, which is the Fourier transform of velocity autocorrelation function $C(t)$, for the case of the 2×2 checkerboard nanoassembly. It can be seen that the dynamical behavior of the confined water and bulk water, as measured by $C(t)$, differs mainly in the subpicosecond regime. Moreover, the density of states of water molecules in between two nanoassemblies is smaller than that of bulk water at the low-frequency regime (0–125 cm^{-1}), indicating again that translational motion of water molecules in between two nanoassemblies is somewhat hindered due to nanoscale confinement. Some additional vibrational motion is also induced for the confined water so that the peak height of $\tilde{C}(\omega)$ increases and the peak position shifts toward higher frequency.

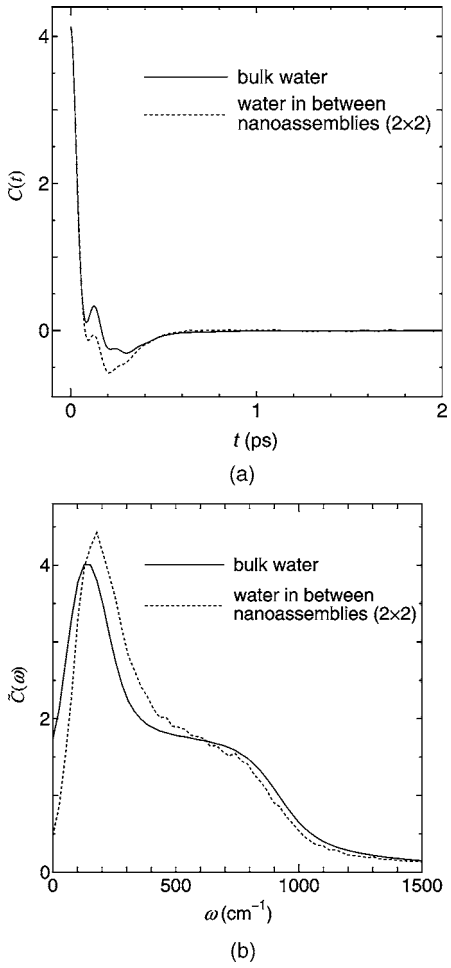

FIG. 9. (a) Calculated velocity autocorrelation function of water in between 2×2 checkerboard nanoassemblies. (b) Calculated density of states of intermolecular vibrational motion of the confined water.

IV. CONCLUSION

In summary, by means of large-scale MD simulations we have gained deeper insight into the physical behavior of midrange nanoscopic hydrophobic interaction through simulation of nanobubble formation between nanometer-sized hydrophobes at constrained equilibrium. We find that the minimum surface area for hydrophobes to sustain a stable nanobubble is likely about 1 nm^2 where a change from short-range molecular hydrophobic interaction to midrange nanoscopic hydrophobic interaction occurs. On the basis of physical behavior of nanobubble formation, we also find that the pattern of nonpolar-site distribution can play an important role to give rise to the nanoscopic hydrophobic interaction, assuming that the total number of nonpolar sites is unchanged. Finally, we find that water molecules diffuses slightly slower in between the 2×2 checkerboard nanoassemblies (having smaller hydrophobic patches) than in between the 3×3 checkerboard nanoassemblies (having larger hydrophobic patches). The relatively, longer lifetime of hydrogen bonds in the confined water (between the two nanoassemblies) in the case of the 2×2 checkerboard model may account for the slower diffusive motion of confined water molecules.

ACKNOWLEDGMENTS

The research is supported by the Japan Ministry of Education, and in part by grants from U.S. DOE (DE-FG02-04ER46164), NSF (DMII/NIRT-0210850 and CHE/ITR-0427746), John Simon Guggenheim Memorial Foundation, and the Nebraska Research Initiative. One of the authors (X.C.Z.) is grateful for valuable discussions with Professors David Chandler, Joan-Emma Shea, and Xueyu Song.

[1] C. Tanford, *The Hydrophobic Effect: Formation of Micelles and Biological Membranes* (Wiley, New York, 1973).
[2] W. Kauzmann, Adv. Protein Chem. **14**, 1 (1959).
[3] K. A. Dill, Biochemistry **29**, 7133 (1990).
[4] D. J. Tobias, J. E. Mertz, and C. L. Brooks, Biochemistry **30**, 6054 (1991).
[5] Y. Duan and P. A. Kollman, Science **282**, 740 (1998).
[6] J. M. Sorenson, G. Hura, A. K. Soper, A. Pertsemlidis, and T. Head-Gordon, J. Phys. Chem. B **103**, 5413 (1999).
[7] A. Suenaga, N. Okimoto, and T. Ebisuzaki, Mol. Simul. **28**, 337 (2002).
[8] L. R. Pratt and D. Chandler, J. Chem. Phys. **67**, 3683 (1977).
[9] C. Pangali, M. Rao, and B. J. Berne, J. Chem. Phys. **71**, 2982 (1979).
[10] K. Watanabe and H. C. Andersen, J. Phys. Chem. **90**, 795 (1986).
[11] D. E. Smith and A. D. J. Haymet, J. Chem. Phys. **98**, 6445 (1993).
[12] L. X. Dang, J. Chem. Phys. **100**, 9032 (1994).
[13] S. Garde, G. Hummer, and M. Paulaitis, Faraday Discuss. **103**, 125 (1996).
[14] L. F. Scatena, M. G. Brown, and G. L. Richmond, Science **292**, 908 (2001).
[15] H. K. Christenson and P. M. Claesson, Science **239**, 390 (1988).
[16] D. R. Berard, P. Attard, and G. N. Patey, J. Chem. Phys. **98**, 7236 (1993).
[17] A. Luzar and K. Leung, J. Chem. Phys. **113**, 5836 (2000).
[18] T. M. Truskett, P. G. Debenedetti, and S. Torquato, J. Chem. Phys. **114**, 2401 (2001).
[19] D. Bratko, R. A. Curtis, H. W. Blanch, and J. M. Prausnitz, J. Chem. Phys. **115**, 3873 (2001).
[20] A. Carambassis, J. C. Jonker, P. Attard, and M. W. Rutland, Phys. Rev. Lett. **80**, 5357 (1998).
[21] X. Y. Zhang, Y. X. Zhu, and S. Granick, J. Am. Chem. Soc. **123**, 6736 (2001).
[22] J. Israelachvili and R. M. Pashley, Nature (London) **300**, 341 (1982).
[23] C. Y. Lee, J. A. McCammon, and P. J. Rossky, J. Chem. Phys. **80**, 4448 (1984).
[24] J. C. Shelley and G. N. Patey, Mol. Phys. **88**, 385 (1996).
[25] K. Lum, D. Chandler, and J. D. Weeks, J. Phys. Chem. B **103**, 4570 (1999).
[26] D. Chandler, Nature (London) **417**, 491 (2002).
[27] F. H. Stillinger, J. Solution Chem. **2**, 141 (1973).
[28] A. Wallqvist and B. J. Berne, J. Phys. Chem. **99**, 2893 (1995).
[29] G. Hummer and S. Garde, Phys. Rev. Lett. **80**, 4193 (1998).
[30] D. M. Huang and D. Chandler, Proc. Natl. Acad. Sci. U.S.A. **97** 8324 (2000).
[31] D. M. Huang, P. L. Geissler, and D. Chandler, J. Phys. Chem. B **105**, 6704 (2001).
[32] X. Huang, C. J. Margulis, and B. J. Berne, Proc. Natl. Acad. Sci. U.S.A. **100**, 11953 (2003).
[33] T. Narumi, R. Susukita, T. Koishi, K. Yasuoka, H. Furusawa, A. Kawai, and T. Ebisuzaki, *Proceedings of SC2000*, Dallas, 2000 (unpublished).
[34] T. Narumi, A. Kawai, and T. Koishi, *Proceedings of SC2001*, Denver, 2001 (unpublished).
[35] T. Koishi, S. Yoo, K. Yasuoka, X. C. Zeng *et al.*, Phys. Rev. Lett. **93**, 185701 (2004).
[36] H. J. C. Beredensen, J. R. Grigera, and T. P. Straatsma, J. Phys. Chem. **91**, 6269 (1987).
[37] W. L. Jorgensen and J. Tirado-Rives, J. Am. Chem. Soc. **110**, 1657 (1988).